DOA Estimation-Based Localization Algorithm for Polarization-Assisted UAV-Borne Radar Systems

Xiaoting Wang, *Graduate Student Member, IEEE*, Xiang Lan, Xianpeng Wang, *Member, IEEE*, Mingcheng Fu, *Member, IEEE*

***Abstract*—Unmanned aerial vehicle (UAV)-borne radar systems have emerged as a core technology for wide-area, high-efficiency target localization and monitoring. However, traditional UAV-borne radar systems are typically configured with uniform linear scalar sensor arrays, in which mutual coupling effects and limited aperture signiffcantly limit the positioning performance. In this paper, a polarization-assisted UAV-borne radar localization system is developed. This system comprises UAVs outfitted with coprime vector sensor arrays. Furthermore, a tensor-based direction-of-arrival (DOA) estimation algorithm leveraging atomic norm minimization (ANM-Tensor-DOA) and a polarization-assisted cross-localization (PACL) technique are introduced. Specifically, an ANM-based optimization task is established based on the cross-correlation matrices of the polarization components to reconstruct the Hermitian Toeplitz-structured noiseless information matrix and the measurement matrix. Subsequently, an augmented noiseless tensor model is established, allowing DOA to be estimated via tensor decomposition. Then the polarization states are determined via closed-form expressions derived from the measurement matrix. Ultimately, based on the known DOA and polarization information, the target's location can be determined using the proposed PACL algorithm. Simulation results indicate that, compared to more recent methods, the proposed approach delivers improved parameter estimation performance and high-precision localization capabilities.**

***Index Terms*—UAV, localization system, coprime EMVS, DOA.**

I. Introduction

UNMANNED aerial vehicles (UAVs), with their flexible maneuverability, low deployment costs, and strong terrain adaptability, have demonstrated significant application potential in various fields such as military reconnaissance, disaster relief, border patrol, and smart cities [1]–[4]. By integrating advanced radar systems, UAVs can become powerful mobile information acquisition nodes, enabling precise detection and localization of specific targets within areas of interest. Estimating the direction-of-arrival (DOA) stands as the cornerstone of localization systems deployed on UAVs. This method utilizes multiple UAVs equipped with sensor arrays to estimate the target's DOA from various spatial perspectives. By integrating the estimated DOA with the UAVs' position data, the target's location coordinates are ultimately determined through triangulation or cross-location techniques [5], [6]. Consequently, the success of localization depends heavily on the precision of DOA estimation. Various DOA estimation algorithms have been proposed for different application scenarios [7]–[10]. For maritime target localization, a system architecture integrating a linear multiple-input multiple-output (MIMO) radar array was designed in [11], and a sparse reconstruction algorithm that accounts for unknown mutual coupling effects was proposed for target's DOA estimation. In [12], [13], vehicle-aided localization algorithms based on DOA estimation were proposed, but the grid mismatch problem was not addressed. Additionally, various neural network models [14], [15] have been proposed. However, these methods are often tailored for specific data types or tasks, resulting in limited generalization ability. Moreover, the aforementioned systems typically employ uniform linear scalar sensor arrays as signal receiving units, where the distance between neighboring sensors must be less than half the signal wavelength. This constraint causes significant mutual coupling among sensors, thereby degrading the accuracy of DOA estimation. At the same time, in challenging environments such as maritime scenarios with severe electromagnetic interference or pronounced anisotropic clutter, as well as urban canyon environments with dense multipath scatters (e.g., buildings and vegetation), scalar sensor arrays are incapable of obtaining accurate DOA.

To tackle the limitation of half-wavelength spacing in conventional uniform arrays, sparse arrays have emerged as a research hotspot [16]–[20]. The classical nested array and coprime array were proposed in [21] and [22], respectively. Such parse arrays adopt non-uniform element spacing, in which the distances between elements are set to integer multiples of the signal's half-wavelength. This configuration significantly expands the effective array aperture and provides a higher degree of freedom (DOF) in the absence of additional physical sensors [23]–[25]. Whereas the nested array has a denser sensor arrangement, the coprime array's sparser configuration leads to less mutual coupling. The vectorized second-order statistics of the measurements from a coprime array can be viewed as a single-snapshot observation of an extended virtual linear array. This facilitates the use of subspace methods like spatial smoothing multiple signal classification (SS-MUSIC) [21] and MUSIC [26], for DOA estimation. However, these algorithms

This work was supported in part by the National Nature Science Foundation of China Youth Science and Fund Project under Grant 62101165; in part by the Scientific Research Setup Fund of Hainan University under Grant KYQD(ZR)-21134.

Xiaoting Wang, Xiang Lan, Xianpeng Wang and Mingcheng Fu are with State Key Laboratory of Marine Resource Utilization in South China Sea and School of Information and Communication Engineering, Hainan University, Haikou 570228, China. (e-mail: wxt@hainanu.edu.cn; xlan@hainanu.edu.cn; wxpeng2016@hainanu.edu.cn; fumcheng@hainanu.edu.cn).

0000–0000/00$00.00 © 2021 IEEE

only make use of the contiguous portion of the difference co-array and discard the non-contiguous virtual apertures, which results in reduced DOF and lower estimation accuracy. To further enhance the DOF, an extended coprime array structure was proposed in [27], which focuses on constructing a virtual linear array with more consecutive virtual elements. Moreover, to fully exploit the entire virtual apertures, co-array interpolation [28], [29] and matrix completion techniques [30]–[32] have been proposed to fill the holes and improve estimation accuracy. However, it should be emphasized that all the studies mentioned above are still fundamentally based on scalar sensor arrays, which are inherently limited in their ability to capture the complete electromagnetic field information.

Electromagnetic vector sensors (EMVSs) are high-performance sensing units widely utilized in signal processing and antenna array systems [33]. They can simultaneously measure both the electric and magnetic field components of an electromagnetic wave along three orthogonal spatial dimensions (x, y, z), thereby providing each source with joint spatial–polarization information. This capability significantly enhances the system's resolution and robustness in complex electromagnetic environments, making EMVSs highly promising for various fields such as mobile communications, electronic reconnaissance, and target recognition [34]. Several conventional parameter estimation algorithms for EMVS arrays, such as eigenspace-based algorithms [35]–[37], compressed sensing [38], [39], as well as quaternion-based methods [40], [41] and tensor decomposition [42], [43] that exploit the multi-dimensional structure information of signals, have been developed. Notably, the focus of these investigations has been predominantly on uniform EMVS arrays, thereby motivating further exploration into non-uniform geometries that could synergistically combine the benefits of sparsity and polarization diversity.

Building on this motivation, the SS-MUSIC algorithm was extended to sparse EMVS arrays in [44], but it only utilizes a portion of the co-array measurements. In [45], a novel co-array interpolation technique was proposed, in which the polarization components of multiple co-array outputs are interpolated separately to construct a higher-dimensional covariance matrix. DOA is then estimated by constructing a nuclear norm minimization (NNM) model and applying the MUSIC algorithm. However, jointly estimating DOA and polarization requires a three-dimensional (3D) spectral peak search, resulting in high computational complexity. To reduce the algorithmic complexity, an efficient co-array interpolation algorithm is proposed in [46]. This algorithm achieves matrix completion by solving an atomic norm minimization (ANM) task, which is constructed based on the measurement matrix. The DOA is then estimated via performing one-dimensional (1D) search, and the polarization parameters are obtained directly from the measurement matrix in the form of closed-form solutions. However, the above two methods achieve hole filling through matrix-level completion techniques, failing to leverage the inherent multidimensional structural information. In [47], the DOA estimation problem for coprime EMVS arrays was addressed from a tensor perspective. However, the DOF remained dependent on the number of physical sensors, resulting in relatively low estimation accuracy. In [48], a tensor model was established for a nested EMVS array, and a Tensor-MUSIC algorithm was proposed. Nevertheless, it did not make full use of all available data from the difference co-array. As a solution, a farallel factor analysis (PARAFAC)-based method was presented in [49], which incorporates all co-array measurements for angle estimation. However, the above two approaches exhibit reduced DOF when applied to coprime EMVS arrays, leading to degraded estimation performance. In [50], a tensor signal model was developed for co-array outputs, and a tensor nuclear norm minimization (TNNM)-based interpolation technique was proposed to avoid aperture loss. However, this approach exhibits poor estimation performance under low signal-to-noise ratio (SNR) conditions.

In this paper, a polarization-assisted UAV-borne radar localization system is developed, which employs a coprime EMVS array configuration. Furthermore, a DOA-based high-precision localization algorithm is developed. The core contributions of this research are outlined below:

1) A tensor-based DOA estimation algorithm via ANM (ANM-Tensor-DOA) is proposed. This method builds a virtual uniform linear array (ULA) by interpolating holes in the physical sensor array, and formulates an ANM problem based on the cross-correlation matrices of the polarization components to reconstruct the Hermitian Toeplitz-structured noiseless information matrix and measurement matrix. Furthermore, a third-order tensor signal model is established based on the interpolated virtual array output, and DOA estimation is achieved through tensor decomposition.
2) The closed-form solutions of polarization estimation are provided, which are derived based on the reconstructed measurement matrices.
3) A polarization-assisted cross-localization (PACL) algorithm is proposed, which utilizes estimated DOAs from multiple UAVs to perform cross-localization for target position determination. For multi-target scenarios, polarization information is utilized to match the estimated DOAs from multiple UAVs, thereby ensuring the accuracy of cross-localization.
4) A series of simulation experiments validate that the proposed algorithm achieves high DOA estimation accuracy and localization precision under challenging conditions, including low SNR, limited snapshots, and the presence of coherent sources.

This paper is organized as follows: Section 2 introduces the system architecture and the signal model; Section 3 details the principles of the developed method; Section 4 presents experiments and analysis under various conditions to validate its effectiveness; Section 5 provides the conclusion.

II. System Architecture and Signal Model

The architecture of the proposed polarization-assisted UAV-borne radar localization system is shown in figure 1. The system consists of multiple UAVs, each equipped with a coprime EMVS array as the signal receiving device, allowing the system to estimate the target's DOA with respect to the

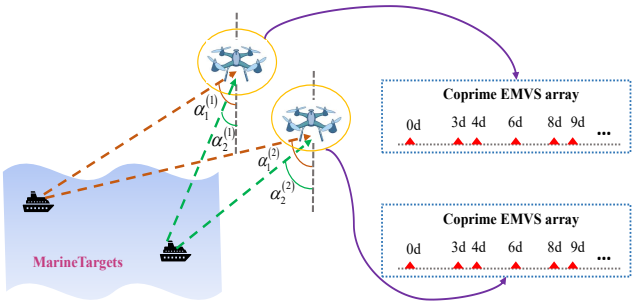

Fig. 1. Localization System Architecture.

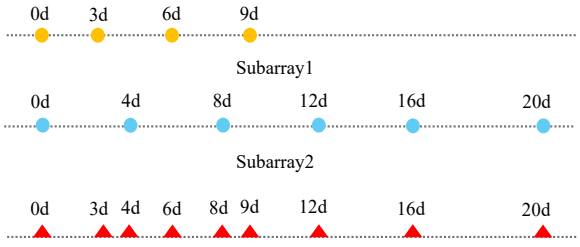

Fig. 2. Coprime EMVS Array Structure ($M = 3, N = 4$).

UAV. The final target localization is achieved by combining the UAV's position (which can be obtained from low Earth orbit satellites) with the target's DOA.

The coprime EMVS array consists of two sparse EMVS subarrays, and the array structure is shown in figure 2. The first subarray contains N elements with a spacing of Md, while the second subarray contains M elements with a spacing of Nd. M and N are coprime numbers, $d = \lambda/2$ represents the distance between adjacent elements, and λ denotes the signal wavelength.

As only the position of the first sensor overlaps in the two subarrays, the coprime EMVS array has a total of $2M+N-1$ sensors, with their positions denoted as $\mathbb{V}d$,where

$$\begin{aligned}\mathbb{V} &= \{v_l \,|l = 1, 2, \cdots, 2M + N - 1\} \\ &= \{Mn \,|0 \le n \le N - 1\} \cup \{Nm \,|0 \le m \le 2M - 1\}.\end{aligned} \tag{1}$$

Since the coprime array is a linear array, we consider only 1D DOA estimation and set the azimuth angle to $0°$. When K fully polarized electromagnetic waves are incident on the array, the received signals can be described as

$$\boldsymbol{y}_{\mathbb{V}}(t) = \sum_{k=1}^{K} (\boldsymbol{a}_{\mathbb{V}}(\theta_k) \otimes \boldsymbol{p}_k) s_k(t) + \boldsymbol{n}_{\mathbb{V}}(t). \tag{2}$$

where the angle parameters of the k-th incident wave are $(\theta_k, \gamma_k, \eta_k)$, representing the elevation angle, polarization auxiliary angle, and polarization phase difference, respectively. $\boldsymbol{a}_{\mathbb{V}}(\theta_k) = \left[e^{-jv_1\varsigma_k}, e^{-jv_2\varsigma_k}, \cdots, e^{-jv_{|\mathbb{V}|}\varsigma_k}\right]^T \in \mathbb{C}^{|\mathbb{V}|}$ is the spatial steering vector, $\varsigma_k = (2\pi d \sin\theta_k)/\lambda$, and $\boldsymbol{n}_{\mathbb{V}}(t)$ is the complex Gaussian white noise vector. $\otimes$ denotes the Kronecker product. $\boldsymbol{p}_k = \boldsymbol{G}_k \boldsymbol{h}_k \in \mathbb{C}^6$ represents the polarization steering vector, where

$$\boldsymbol{G}_k = \begin{bmatrix} \cos(\theta_k) & 0 \\ 0 & 1 \\ -\sin(\theta_k) & 0 \\ 0 & -\cos(\theta_k) \\ 1 & 0 \\ 0 & \sin(\theta_k) \end{bmatrix}. \tag{3}$$

$$\boldsymbol{h}_k = \begin{bmatrix} \sin(\gamma_k)\, e^{j\eta_k} \\ \cos(\gamma_k) \end{bmatrix}. \tag{4}$$

III. Proposed Algorithms

In this section, an ANM-Tensor-DOA estimation algorithm and a PACL algorithm are proposed for the UAV-borne coprime EMVS array positioning system to achieve accurate target localization.

A. ANM-Tensor-DOA Algorithm

The algorithm first reconstructs the Hermitian Toeplitz-structured noiseless information matrix and measurement matrix by solving the ANM problem associated with the cross-correlation matrices of the polarization components, thereby filling the holes. Then, an augmented noiseless tensor model is established, and DOA estimation is achieved through tensor decomposition. Polarization parameters are estimated using the closed-form solutions derived from the measurement matrix.

According to (2), the i-th polarization component output by the coprime EMVS array is formulated as

$$\boldsymbol{x}_{\mathbb{V},i}(t) = \sum_{k=1}^{K} p_{k,i} \boldsymbol{a}_{\mathbb{V}}(\theta_k) s_k(t) + \boldsymbol{n}_{\mathbb{V},i}(t). \tag{5}$$

where $p_{k,i}$ corresponds to the i-th element of the vector $\boldsymbol{p}_k$, $i = 1, 2, \cdots, 6$, and $\boldsymbol{n}_{\mathbb{V},i}(t)$ represents the additive noise vector of the polarization component. As shown in figure 2, the coprime array exhibits a highly sparse element distribution. By interpolating the hole positions, a virtual ULA array that matches the Nyquist sampling theorem can be obtained, with the set of sensor positions denoted as $\mathbb{U}d$

$$\mathbb{U} = \{u \,|0 \le u \le \max(\mathbb{V})\}. \tag{6}$$

The i-th polarization component of the virtual ULA output is

$$\begin{aligned}\boldsymbol{x}_{\mathbb{U},i}(t) &= \sum_{k=1}^{K} p_{k,i} \boldsymbol{a}_{\mathbb{U}}(\theta_k) s_k(t) + \boldsymbol{n}_{\mathbb{U},i}(t) \\ &= \boldsymbol{A}_{\mathbb{U}} \boldsymbol{f}_i + \boldsymbol{n}_{\mathbb{U},i}(t).\end{aligned} \tag{7}$$

where $\boldsymbol{f}_i = [f_{1,i}, f_{2,i}, \cdots, f_{K,i}]^T$, $f_{k,\mathrm{i}} = p_{k,i} s_k(t)$, $\boldsymbol{A}_{\mathbb{U}} = [\boldsymbol{a}_{\mathbb{U}}(\theta_1), \boldsymbol{a}_{\mathbb{U}}(\theta_2), \cdots, \boldsymbol{a}_{\mathbb{U}}(\theta_K)] \in \mathbb{C}^{|\mathbb{U}|\times K}$, The cross-correlation matrix between the i-th polarization component and the j-th ($j = 1, 2, \cdots, 6$) polarization component is represented as

$$\boldsymbol{R}_{\mathbb{U},ij} = E\left\{\boldsymbol{x}_{\mathbb{U},i}\left(t\right)\boldsymbol{x}_{\mathbb{U},j}^{H}\left(t\right)\right\} = \boldsymbol{A}_{\mathbb{U}}\boldsymbol{f}_i\boldsymbol{f}_j^{H}\boldsymbol{A}_{\mathbb{U}}^{H} + \sigma_n^2\boldsymbol{I}. \quad (8)$$

where σ_n^2 denotes the noise variance, and $\boldsymbol{I} \in \mathbb{C}^{|\mathbb{U}|\times|\mathbb{U}|}$ denotes the identity matrix. Define the selection matrix $\boldsymbol{J} = \left[\boldsymbol{e}_1, \boldsymbol{e}_2, \cdots, \boldsymbol{e}_{|\mathbb{V}|}\right] \in \mathbb{C}^{|\mathbb{U}|\times|\mathbb{V}|}$, where $\boldsymbol{e}_l$ is a column vector with the (v_l+1)-th element equal to 1 and all other elements equal to 0. The non-zero columns of $\boldsymbol{R}_{\mathbb{U},ij}$ are selected as

$$\begin{aligned}\boldsymbol{R}_{ij} &= \boldsymbol{R}_{\mathbb{U},ij}\boldsymbol{J}\\ &= \boldsymbol{A}_{\mathbb{U}}\boldsymbol{f}_i\boldsymbol{f}_j^{H}\boldsymbol{A}_{\mathbb{U}}^{H}\boldsymbol{J} + \sigma_n^2\boldsymbol{J}\\ &= \widetilde{\boldsymbol{R}}_{ij} + \sigma_n^2\boldsymbol{J}\\ &= \boldsymbol{A}_{\mathbb{U}}\boldsymbol{Q}_{ij} + \sigma_n^2\boldsymbol{J}\\ &= \sum_{k=1}^{K}\boldsymbol{a}_{\mathbb{U}}\left(\theta_k\right)\boldsymbol{q}_{k,ij} + \sigma_n^2\boldsymbol{J}. \end{aligned} \quad (9)$$

where $\boldsymbol{Q}_{ij} = \left[\boldsymbol{q}_{1,ij}^T, \boldsymbol{q}_{2,ij}^T, \ldots, \boldsymbol{q}_{K,ij}^T\right]^T \in \mathbb{C}^{K\times|\mathbb{V}|}$, $\boldsymbol{q}_{k,ij} = f_{k,i}\boldsymbol{f}_j^{H}\boldsymbol{A}_{\mathbb{V}}^{H} = \sigma_k^2 p_{k,i}p_{k,j}^{*}\boldsymbol{a}_{\mathbb{V}}^{H}\left(\theta_k\right)$, $\sigma_k^2 = E\left\{s_k\left(t\right)s_k^{*}\left(t\right)\right\}$ is the power associated with the k-th signal. $\widetilde{\boldsymbol{R}}_{ij}$ can be further expressed as

$$\widetilde{\boldsymbol{R}}_{ij} = \sum_{k=1}^{K} c_{k,ij}\boldsymbol{a}_{\mathbb{U}}\left(\theta_k\right)\boldsymbol{b}_{k,ij}. \quad (10)$$

where $c_{k,ij} = \left\|\boldsymbol{q}_{k,ij}\right\|_2 > 0$, $\boldsymbol{b}_{k,ij} = c_{k,ij}^{-1}\boldsymbol{q}_{k,ij}$, $\left\|\boldsymbol{b}_{k,ij}\right\|_2 = 1$. $\widetilde{\boldsymbol{R}}_{ij}$ can be described by the atomic set

$$\mathcal{A} = \left\{\boldsymbol{a}_{\mathbb{U}}\left(\theta\right)\boldsymbol{b}_{ij}\,\middle|\,\theta\in\left[-\frac{\pi}{2},\frac{\pi}{2}\right], \boldsymbol{b}_{ij}\in{}^{1\times|\mathbb{V}|}, \left\|\boldsymbol{b}_{ij}\right\|_2 = 1\right\}. \quad (11)$$

The atomic l_0-norm of $\widetilde{\boldsymbol{R}}_{ij}$ refers to the minimum number of atoms in $\mathcal{A}$

$$\left\|\widetilde{\boldsymbol{R}}_{ij}\right\|_{\mathcal{A},0} = \inf_{\mathcal{K}}\left\{\widetilde{\boldsymbol{R}}_{ij} = \sum_{k=1}^{\mathcal{K}} c_{k,ij}\boldsymbol{a}_{\mathbb{U}}\left(\theta_k\right)\boldsymbol{b}_{k,ij}, c_{k,ij} > 0\right\}. \quad (12)$$

where inf represents the infimum. Given that minimizing the above problem is NP-hard, we turn to the convex relaxation of $\left\|\widetilde{\boldsymbol{R}}_{ij}\right\|_{\mathcal{A},0}$

$$\begin{aligned}\left\|\widetilde{\boldsymbol{R}}_{ij}\right\|_{\mathcal{A}} &= \inf\left\{\tau > 0 : \widetilde{\boldsymbol{R}}_{ij}\in\tau\mathrm{conv}\left(\mathcal{A}\right)\right\}\\ &= \inf\left\{\sum_k \mathrm{c}_{k,ij}\,\middle|\,\widetilde{\boldsymbol{R}}_{ij} = \sum\nolimits_k c_{k,ij}\boldsymbol{a}_{\mathbb{U}}\left(\theta_k\right)\boldsymbol{b}_{k,ij}, c_{k,ij} > 0\right\}.\end{aligned} \quad (13)$$

where $\mathrm{conv}\left(\mathcal{A}\right)$ denotes the convex hull of $\mathcal{A}$. The i-th polarization component of the virtual ULA output is initialized to

$$\left\langle\widetilde{\boldsymbol{x}}_{\mathbb{U},i}\left(t\right)\right\rangle_\ell = \begin{cases}\left\langle\boldsymbol{x}_{\mathbb{V},i}\left(t\right)\right\rangle_\ell, \ell\in\mathbb{V}\\ 0, \ell\in\mathbb{U}\backslash\mathbb{V}\end{cases}. \quad (14)$$

where $\left\langle\boldsymbol{x}\right\rangle_\ell$ represents the element of vector $\boldsymbol{x}$ at index ℓ, and $\ell\in\mathbb{U}\backslash\mathbb{V}$ indicates that ℓ belongs to $\mathbb{U}$ but not to $\mathbb{V}$. The sampled cross-correlation matrix between the i-th and j-th polarization components is given by

$$\widehat{\boldsymbol{R}}_{\mathbb{U},ij} = \frac{1}{T}\sum_{t=1}^{T}\widetilde{\boldsymbol{x}}_{\mathbb{U},i}\left(t\right)\widetilde{\boldsymbol{x}}_{\mathbb{U},j}^{H}\left(t\right). \quad (15)$$

where T denotes the number of snapshoots. The non-zero columns of $\widehat{\boldsymbol{R}}_{\mathbb{U},ij}$ are then extracted as

$$\widehat{\boldsymbol{R}}_{ij} = \widehat{\boldsymbol{R}}_{\mathbb{U},ij}\boldsymbol{J}. \quad (16)$$

Due to the interpolation operation, $\widehat{\boldsymbol{R}}_{ij}$ contains several zero rows. The missing entries can be completed by addressing the ANM task

$$\min_{\widetilde{\boldsymbol{R}}_{ij}}\mu\left\|\widetilde{\boldsymbol{R}}_{ij}\right\|_{\mathcal{A}} + \frac{1}{2}\left\|\widetilde{\boldsymbol{R}}_{ij}\oplus\boldsymbol{Z} - \widehat{\boldsymbol{R}}_{ij}\right\|_F^2. \quad (17)$$

where μ is the regularization parameter, $\oplus$ denotes the Hadamard product. $\boldsymbol{Z}\in\mathbb{C}^{|\mathbb{U}|\times|\mathbb{V}|}$ is a binary matrix where the entries corresponding to the non-zero rows of $\widehat{\boldsymbol{R}}_{ij}$ are 1, while all other rows are 0. The above problem can be reformulated as a Semi-Definite Programming (SDP) problem

$$\begin{aligned}&\min_{\boldsymbol{D},\boldsymbol{z},\widetilde{\boldsymbol{R}}_{ij}}\ \frac{\mu}{2|\mathbb{U}|}\left[tr\left(\boldsymbol{D}\right) + tr\left(\mathcal{T}\left(\boldsymbol{z}_{ij}\right)\right)\right] + \frac{1}{2}\left\|\widetilde{\boldsymbol{R}}_{ij}\oplus\boldsymbol{Z} - \widehat{\boldsymbol{R}}_{ij}\right\|_F^2\\ &\text{subject to}\quad \begin{bmatrix}\boldsymbol{D} & \widetilde{\boldsymbol{R}}_{ij}^{H}\\ \widetilde{\boldsymbol{R}}_{ij} & \mathcal{T}\left(\boldsymbol{z}_{ij}\right)\end{bmatrix}\succeq 0\end{aligned}. \quad (18)$$

where $\boldsymbol{D}\in\mathbb{C}^{|\mathbb{V}|\times|\mathbb{V}|}$ is a Hermitian matrix, and $\mathcal{T}\left(\boldsymbol{z}_{ij}\right)\in\mathbb{C}^{|\mathbb{U}|\times|\mathbb{U}|}$ is a Hermitian Toeplitz matrix constructed from the first column $\boldsymbol{z}_{ij} = \sum_{k=1}^{K} c_{k,ij}\boldsymbol{a}_{\mathbb{U}}\left(\theta_k\right)$, with the following structure

$$\mathcal{T}\left(\boldsymbol{z}_{ij}\right) = \boldsymbol{A}_{\mathbb{U}}\boldsymbol{\Lambda}_{ij}\boldsymbol{A}_{\mathbb{U}}^{H} = \sum_{k=1}^{K} c_{k,ij}\boldsymbol{a}_{\mathbb{U}}\left(\theta_k\right)\boldsymbol{a}_{\mathbb{U}}^{H}\left(\theta_k\right). \quad (19)$$

where

$$\boldsymbol{\Lambda}_{ij} = \mathrm{diag}\left(\left[c_{1,ij}, \cdots, c_{K,ij}\right]\right). \quad (20)$$

After solving problem (18), the 36 matrices $\mathcal{T}\left(\boldsymbol{z}_{ij}\right)$ can be arranged into a third-order tensor, which is expressed as

$$\begin{aligned}\boldsymbol{T} &= \left[\mathcal{T}\left(\boldsymbol{z}_{11}\right), \mathcal{T}\left(\boldsymbol{z}_{12}\right), \cdots, \mathcal{T}\left(\boldsymbol{z}_{61}\right), \cdots, \mathcal{T}\left(\boldsymbol{z}_{66}\right)\right]_{\sqcup_3}\\ &= \sum_{k=1}^{K} r_k\boldsymbol{a}_{\mathbb{U}}\left(\theta_k\right)\circ\boldsymbol{a}_{\mathbb{U}}^{*}\left(\theta_k\right)\circ\overline{\boldsymbol{d}}_k.\end{aligned} \quad (21)$$

where $r_k = |\mathbb{V}|\,\delta_k^4$, $\overline{\boldsymbol{d}}_k = \boldsymbol{d}_k\otimes\boldsymbol{d}_k$, $\boldsymbol{d}_k = \boldsymbol{p}_k\oplus\boldsymbol{p}_k^{*}$, $\circ$ represents the outer product, and $\left[\bullet\right]_{\sqcup_3}$ denotes concatenation along the third dimension. By performing tensor decomposition on $\boldsymbol{T}$, we can obtain the factor matrices $\boldsymbol{A}_{\mathbb{U}}$, $\boldsymbol{A}_{\mathbb{U}}^{*}$, and $\overline{\boldsymbol{D}}$, where $\boldsymbol{A}_{\mathbb{U}}$ is the spatial steering factor matrix, which incorporates the DOA of the sources, $\overline{\boldsymbol{D}} = \left[\overline{\boldsymbol{d}}_1, \overline{\boldsymbol{d}}_2, \cdots, \overline{\boldsymbol{d}}_K\right]\in\mathbb{C}^{36\times K}$.

Theorem 1: When $K\le\left|\mathbb{U}\right|$, the following inequality holds

$$k_{\boldsymbol{A}_{\mathbb{U}}} + k_{\boldsymbol{A}_{\mathbb{U}}^{*}} + k_{\overline{\boldsymbol{D}}} \ge 2K + 2. \quad (22)$$

Proof 1: Since $\boldsymbol{a}_{\mathbb{U}}(\theta_k)$ has a Vandermonde structure, it follows that $k_{\boldsymbol{A}_{\mathbb{U}}} = k_{\boldsymbol{A}_{\mathbb{U}}^*} = \min(K, |\mathbb{U}|)$. Let $\overline{\boldsymbol{D}}$ be represented as $\overline{\boldsymbol{D}} = \boldsymbol{D} \odot \boldsymbol{D}$, $\boldsymbol{D} = [\boldsymbol{d}_1, \boldsymbol{d}_2, \cdots \boldsymbol{d}_K]$. According to Lemma 1 in [51], any two columns of $\boldsymbol{D}$ are also linearly independent. Therefore, $k_{\boldsymbol{D}} \geq 2$, and further, $k_{\overline{\boldsymbol{D}}} \geq 2$. Hence, when $K \leq |\mathbb{U}|$, (22) holds, and Theorem 1 is proven.

According to Theorem 1, the factor matrices obtained by performing a tensor decomposition on $\boldsymbol{T}$ are unique, but there exist permutation and scale ambiguities. Permutation ambiguity refers to the change in the order of the columns in the factor matrices, while scale ambiguity refers to the scaling of the amplitude of each column by a constant factor. The perturbation of the factor matrix $\boldsymbol{A}_{\mathbb{U}}$ due to these ambiguities can be modeled as

$$\widehat{\boldsymbol{A}}_{\mathbb{U}} = \boldsymbol{A}_{\mathbb{U}} \Pi \Delta + \boldsymbol{N}. \tag{23}$$

where Π is a permutation matrix, Δ is a diagonal matrix, and $\boldsymbol{N}$ represents the fitting error. The k-th column of matrix $\widehat{\boldsymbol{A}}_{\mathbb{U}}$ corresponds to the estimated steering vector for the k-th target

$$\widehat{\boldsymbol{a}}_{\mathbb{U}}(\theta_k) = \left[1, e^{-j2\pi d \sin\theta_k/\lambda}, \cdots, e^{-j\max(\mathbb{V})2\pi d \sin\theta_k/\lambda}\right]^T. \tag{24}$$

Obviously, the DOA information can be extracted from the phase of $\widehat{\boldsymbol{a}}_{\mathbb{U}}(\theta_k)$

$$\widehat{\theta}_k = \arcsin\left(\boldsymbol{v}^{-1}\boldsymbol{\omega}_k\right). \tag{25}$$

where $\boldsymbol{v} = -\pi[0, 1, \cdots, \max(\mathbb{V})]^T$, $\boldsymbol{\omega}_k = \text{angle}\left(\widehat{\boldsymbol{a}}_{\mathbb{U}}(\theta_{\text{k}})\right)$.

B. Polarization Estimation

The polarization parameters can be obtained from the recovered measurement matrix $\widetilde{\boldsymbol{R}}_{ij}$, According to (9), we know that

$$\widetilde{\boldsymbol{R}}_{ij} = \widehat{\boldsymbol{A}}_{\mathbb{U}} \boldsymbol{Q}_{ij}. \tag{26}$$

Therefore, $\boldsymbol{Q}_{ij}$ can be estimated by solving the following optimization problem

$$\min_{\boldsymbol{Q}_{ij}} \left\| \widetilde{\boldsymbol{R}}_{ij} - \widehat{\boldsymbol{A}}_{\mathbb{U}} \boldsymbol{Q}_{ij} \right\|_F. \tag{27}$$

The solution to problem (27) is

$$\widehat{\boldsymbol{Q}}_{ij} = \left(\widehat{\boldsymbol{A}}_{\mathbb{U}}^H \widehat{\boldsymbol{A}}_{\mathbb{U}}\right)^{-1} \widehat{\boldsymbol{A}}_{\mathbb{U}}^H \widetilde{\boldsymbol{R}}_{ij}. \tag{28}$$

The k-th row of $\widehat{\boldsymbol{Q}}_{ij}$ is represented as

$$\widehat{\boldsymbol{q}}_{k,ij} = [\boldsymbol{\rho}_k]_{6(j-1)+i} \boldsymbol{a}_{\mathbb{V}}^H\left(\widehat{\theta}_k\right). \tag{29}$$

where $[\bullet]_n$ represents the n-th element of the vector, and

$$\boldsymbol{\rho}_k = \sigma_k^2 \overline{\boldsymbol{p}}_k = \sigma_k^2 \left(\boldsymbol{p}_k^* \otimes \boldsymbol{p}_k\right) = \left(\boldsymbol{G}_k^* \otimes \boldsymbol{G}_k\right) \boldsymbol{\upsilon}_k. \tag{30}$$

where $\boldsymbol{\upsilon}_k = \sigma_k^2 \overline{\boldsymbol{h}}_k$,

$$\begin{aligned} \overline{\boldsymbol{h}}_k &= \left(\boldsymbol{h}_k^* \otimes \boldsymbol{h}_k\right) \\ &= \left[\sin^2\gamma_k \sin\gamma_k \cos\gamma_k e^{-j\eta_k}, \sin\gamma_k \cos\gamma_k e^{j\eta_k}, \cos^2\gamma_k\right]. \end{aligned} \tag{31}$$

It is evident that $\left\|\overline{\boldsymbol{h}}_k\right\|_2 = 1$, and thus, $\overline{\boldsymbol{h}}_k = \boldsymbol{\upsilon}_k / \|\boldsymbol{\upsilon}_k\|_2$. According to (29), we can obtain the estimation $\widehat{\boldsymbol{\rho}}_k$ of $\boldsymbol{\rho}_k$ by iterating over all values of i and j. Furthermore, we can obtain the estimation of $\overline{\boldsymbol{h}}_k$

$$\widehat{\overline{\boldsymbol{h}}}_k = \widehat{\boldsymbol{\upsilon}}_k / \|\widehat{\boldsymbol{\upsilon}}_k\|_2. \tag{32}$$

where

$$\widehat{\boldsymbol{\upsilon}}_k = \left(\widehat{\boldsymbol{G}}_k^* \otimes \widehat{\boldsymbol{G}}_k\right)^{\dagger} \widehat{\boldsymbol{\rho}}_k. \tag{33}$$

Finally, the polarization parameters are estimated via

$$\widehat{\gamma}_k = \tan^{-1}\left(\left|\frac{\left[\widehat{\overline{\boldsymbol{h}}}_k\right]_3}{\left[\widehat{\overline{\boldsymbol{h}}}_k\right]_4}\right|\right). \tag{34}$$

$$\widehat{\eta}_k = \arg\left(\left|\frac{\left[\widehat{\overline{\boldsymbol{h}}}_k\right]_1}{\left[\widehat{\overline{\boldsymbol{h}}}_k\right]_2}\right|\right). \tag{35}$$

Table I summarises the implementation process of the proposed algorithm.

TABLE I
DESCRIPTION OF THE ANM-TENSOR-DOA ESTIMATION ALGORITHM

ANM-Tensor-DOA Estimation Algorithm
1. Extract the polarization component $\boldsymbol{x}_{\mathbb{V},i}$ according to (5).
2. Initialize the output polarization component $\widetilde{\boldsymbol{x}}_{\mathbb{U},i}$ of the virtual ULA based on (14).
3. Compute the cross-correlation matrix $\widehat{\boldsymbol{R}}_{\mathbb{U},ij}$ via (15).
4. Select the non-zero columns $\widehat{\boldsymbol{R}}_{ij}$ of $\widehat{\boldsymbol{R}}_{\mathbb{U},ij}$ according to (16).
5. Solve (18) to obtain $\mathcal{T}(\boldsymbol{z}_{ij})$.
6. Construct the tensor model according to (21).
7. Perform tensor decomposition to obtain $\widehat{\boldsymbol{A}}_{\mathbb{U}}$.
8. Estimate the DOA based on (25).
9. Calculate $\widehat{\boldsymbol{Q}}_{ij}$ via (28), then sequentially obtain $\widehat{\boldsymbol{\rho}}_k$, $\widehat{\boldsymbol{\upsilon}}_k$, $\widehat{\overline{\boldsymbol{h}}}_k$ via (29), (33) and (32), respectively.
10. Estimate the polarization parameters according to (34) and (35).

C. PACL Algorithm

In this section, a PACL algorithm is introduced for multi-target localization. The algorithm first utilizes the estimated polarization parameters to match the DOAs obtained from multiple UAVs. Then, based on the coordinates of the UAVs and the estimated DOAs for the same target, cross-localization is performed to ultimately determine the target's position. A minimum of two UAVs is required to achieve cross positioning, while the positioning accuracy is affected by their geometric configuration when more than two UAVs are deployed. Therefore, to clarify the algorithm procedure, we only take a positioning system composed of two UAVs (UAV1 and UAV2) as an example for illustration.

The planar structure of the localization system is shown in figure 3. The positions of the two UAVs are given by UAV1: $(b_1, 0)$ and UAV2: $(0, b_2)$. Assume there are two targets, T_1 and T_2, located at positions (x_1, y_1) and (x_2, y_2), respectively.

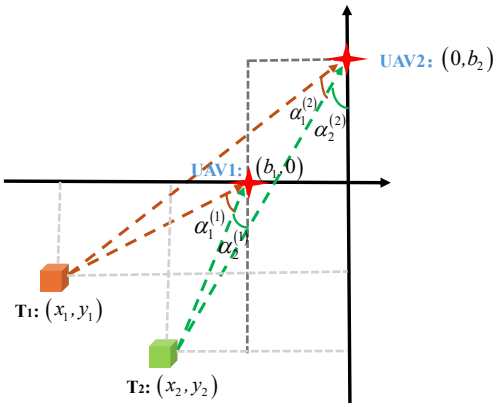

Fig. 3. Planar Structure of the Localization System.

The DOAs of T_1 relative to UAV1 and UAV2 are denoted as $\alpha_1^{(1)}$ and $\alpha_1^{(2)}$, while the DOAs of T_2 relative to UAV1 and UAV2 are $\alpha_2^{(1)}$ and $\alpha_2^{(2)}$, respectively. The superscript indicates the UAV index, and the subscript denotes the target index. Assuming both the targets and UAVs lie in the two-dimensional (2D) Cartesian coordinate plane, the following geometric relationships hold for T_1

$$\begin{cases} \tan\alpha_1^{(1)} = -\frac{x_1-b_1}{y_1} \\ \tan\alpha_1^{(2)} = -\frac{x_1}{y_1-b_2} \end{cases}. \tag{36}$$

Similarly, for T_2, we have

$$\begin{cases} \tan\alpha_2^{(1)} = -\frac{x_2-b_1}{y_2} \\ \tan\alpha_2^{(2)} = -\frac{x_2}{y_2-b_2} \end{cases}. \tag{37}$$

The polarization information about T_1 and T_2 provided by UAV1 are denoted as $\left(\gamma_1^{(1)},\eta_1^{(1)}\right)$ and $\left(\gamma_2^{(1)},\eta_2^{(1)}\right)$ respectively, while the polarization information about T_1 and T_2 provided by UAV2 are denoted as $\left(\gamma_1^{(2)},\eta_1^{(2)}\right)$ and $\left(\gamma_2^{(2)},\eta_2^{(2)}\right)$, respectively. To ensure the accuracy of cross-localization, for T_1, target matching can be achieved by comparing the Euclidean distance between $\left(\gamma_1^{(1)},\eta_1^{(1)}\right)$ and $\left(\gamma_1^{(2)},\eta_1^{(2)}\right)$ with that between $\left(\gamma_1^{(1)},\eta_1^{(1)}\right)$ and $\left(\gamma_2^{(2)},\eta_2^{(2)}\right)$. Assuming the above representations are already matched, i.e., $\left(\gamma_1^{(1)},\eta_1^{(1)}\right)$ and $\left(\gamma_1^{(2)},\eta_1^{(2)}\right)$ correspond to the same target T_1, the cross-localization result for T_1 is given by

$$\begin{cases} x_1 = \dfrac{b_1\tan\alpha_1^{(2)} - b_2\tan\alpha_1^{(2)}\tan\alpha_1^{(1)}}{\tan\alpha_1^{(2)} - \tan\alpha_1^{(1)}} \\ y_1 = \dfrac{b_2\tan\alpha_1^{(2)} - b_1}{\tan\alpha_1^{(2)} - \tan\alpha_1^{(1)}} \end{cases}. \tag{38}$$

Similarly, the position of T_2 can be obtained through the same process.

D. Complexity Analysis

The main content of this section involves discussing the complexity of the DOA estimation process and making a comparison with the ANM [46] and TNNM [50] algorithms. The proposed algorithm's complexity is primarily driven by solving the SDP problem and carrying out tensor decomposition, giving an overall complexity of $O(36(2MN+2M)^{3.5}+2(2MN-N+1)^3+36^3+(4MN-2N+38)K^2)$. For the ANM algorithm, the main complexity comes from solving the SDP problem and executing the 1D spectral search, leading to an overall complexity of $O((4MN-2N+1+36)^{3.5}+\frac{4}{3}(4MN-2N+1)^3+S_\theta(4MN-2N+1)^2)$. The TNNM algorithm's complexity is largely determined by solving the TNNM problem and performing tensor decomposition, with an approximate total complexity of $O(36(2MN-N+1)^3+2(2MN-N+1)^3+36^3+(4MN-2N+38)K^2)$. When compared to the ANM algorithm, the proposed algorithm demonstrates reduced complexity.

IV. Simulation Experiments

In this part, we analyze the proposed algorithm's estimation effectiveness from multiple aspects, including different SNRs, varying numbers of snapshots, and the presence of coherent sources. We also compare the results with the ANM algorithm [46], TNNM algorithm [50], OGSR algorithm [52] and the CRB [33]. The co-prime EMVS array configured for a single UAV consists of two sparse subarrays with element numbers $2M=6$ and $N=4$, respectively. First, we evaluate the ability of a single UAV to estimate DOA in different scenarios. Then, we evaluate the accuracy of the localization system consisting of two UAVs for maritime multi-target localization. Suppose two signals of equal power are incident upon the EMVS array from directions $(\theta_1,\gamma_1,\eta_1)=(10.4^\circ,20.5^\circ,30.2^\circ)$ and $(\theta_2,\gamma_2,\eta_2)=(24.7^\circ,40.8^\circ,50.5^\circ)$, azimuth angle is 90°. The regularization parameter for the proposed algorithm is set to $\mu=1$ and the search step size for the ANM algorithm is 0.5°. All experimental results are the averages of 100 Monte Carlo simulations.

A. DOA and Polarization Estimation

When two target signals are uncorrelated, we observed the DOA estimation performance of several algorithms under seven different SNR levels $SNR=\{-10,-5,0,5,10,15,20\}\,dB$, with $T=200$ snapshots. The results are presented in figure 4. In the range from -5dB to 20dB, the TNNM algorithm demonstrates a lower estimation error than the ANM algorithm. This can be attributed to the TNNM algorithm's exploitation of the multi-dimensional structure of the EMVS array, leading to improved DOA estimation accuracy to some extent. As the SNR decreases to -10dB, the TNNM algorithm's estimation error grows. The OGSR algorithm estimates the DOA from a sparse reconstruction perspective and shows higher estimation accuracy under high SNR conditions. However, across the entire SNR range, the estimation accuracy of our method is significantly higher than that of the comparison methods.

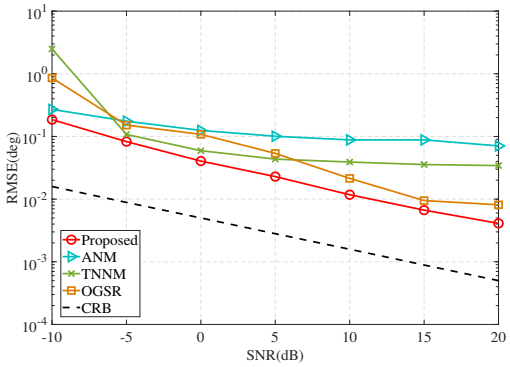

Fig. 4. RMSE of DOA for uncorrelated sources versus SNR.

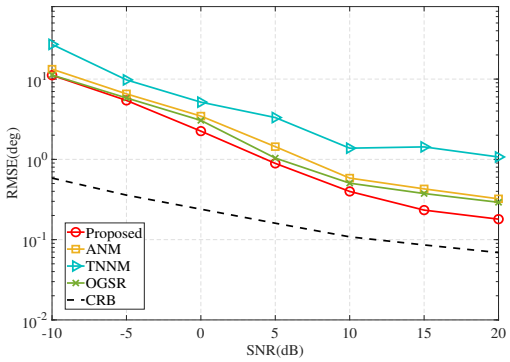

Fig. 5. RMSE of γ for uncorrelated sources versus SNR.

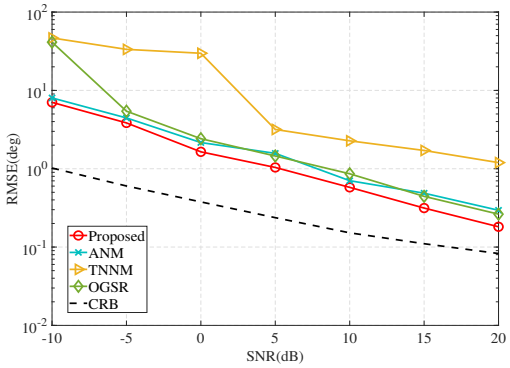

Fig. 6. RMSE of η for uncorrelated sources versus SNR.

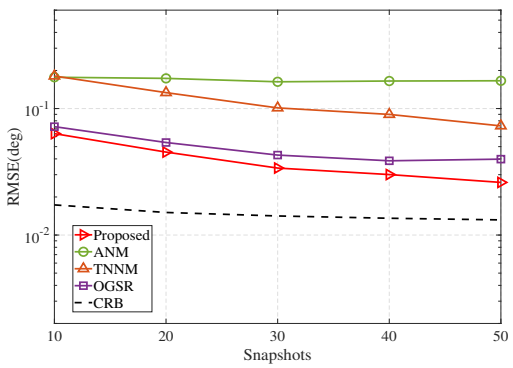

Fig. 7. RMSE of DOA for uncorrelated sources versus snapshots.

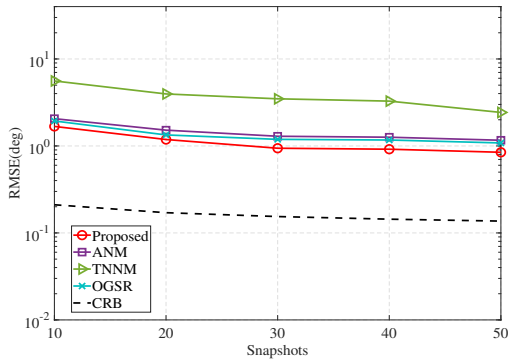

Fig. 8. RMSE of γ for uncorrelated sources versus snapshots.

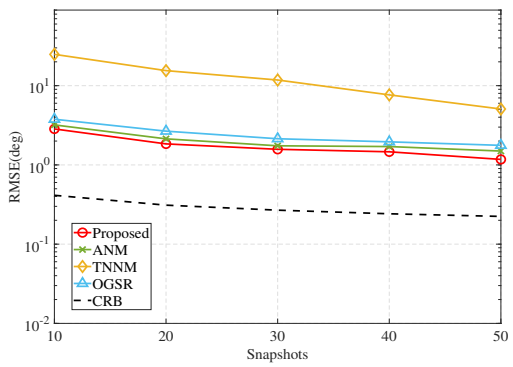

Fig. 9. RMSE of η for uncorrelated sources versus snapshots.

Figure 5 and figure 6 display the corresponding polarization estimation results. At low SNRs (-10dB, -5dB), the proposed algorithm provides similar estimation accuracy for γ as the ANM and OGSR algorithms. However, when the SNR exceeds -5dB, the advantage of the proposed algorithm becomes more pronounced. Furthermore, our algorithm provides a more accurate estimation for η than the three algorithms used for comparison.

Figure 7 illustrates the impact of varying numbers of snapshots $T = \{10, 20, 30, 40, 50\}$ on the DOA estimation performance, with an SNR of 10dB. As shown, in comparison with the ANM, TNNM, and OGSR algorithms, our method consistently maintains a lower RMSE across various snapshots, indicating its excellent robustness under limited snapshots. The corresponding estimation result for γ are shown in figure 8, while the result for η are presented in figure 9. Clearly, the RMSE of the proposed method for polarization estimation follows a similar trend to that for DOA estimation with the number of snapshots, while consistently remaining lower than those of the three comparison algorithms. This further validates the strong robustness of the proposed algorithm for joint parameter estimation under limited snapshot conditions.

When the target signals are coherent, figure 10, figure 11,

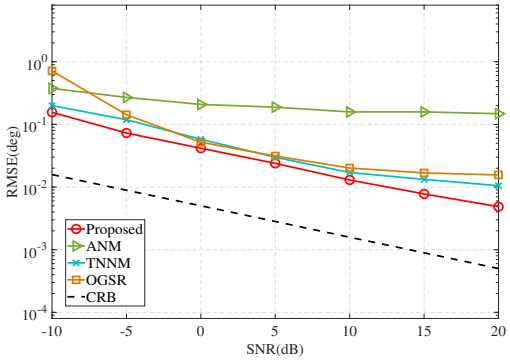

Fig. 10. RMSE of DOA for coherent sources versus SNR.

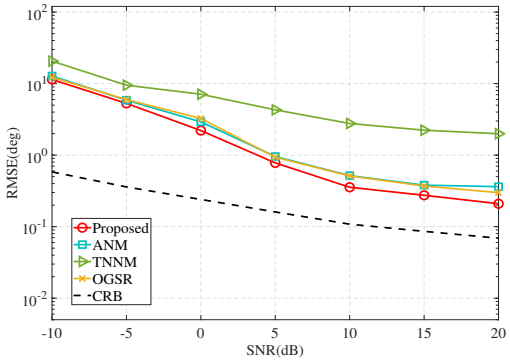

Fig. 11. RMSE of γ for coherent sources versus SNR.

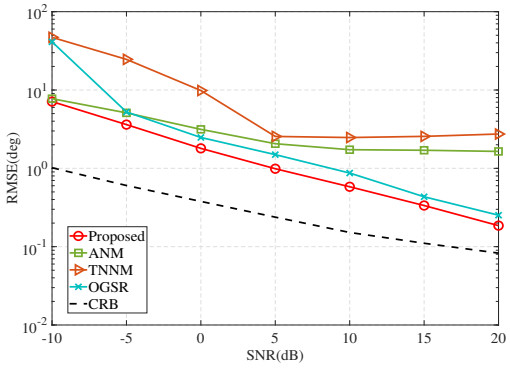

Fig. 12. RMSE of η for coherent sources versus SNR.

and figure 12 display the estimation results for DOA and polarization parameters (γ, η) by several algorithms. Figure 10 illustrates that coherence significantly degrades the DOA estimation accuracy of the ANM algorithm, whereas our method maintains stable estimation performance with consistently higher accuracy than the TNNM and OGSR algorithms. The proposed algorithm also exhibits comparable advantages in polarization estimation, demonstrating robust performance in coherent environments.

TABLE II
LOCALIZATION ERRORS OF THE ALGORITHMS

Method	0dB (AE/m)	10dB (AE/m)
Proposed	8.1561	2.2771
ANM	11.7696	9.0738
TNNM	10.4795	9.3006
OGSR	12.8292	3.0108

B. Target Localization

From the previous analysis, it is clear that the accuracy of localization primarily depends on the precision of the DOA estimation. Therefore, in this section, we compare and analyze the localization performance of several algorithms. The position parameters of the UAVs and the targets are set as $b_1 = -500m$, $b_2 = 600m$, $(x_1, y_1) = (-600m, -800m)$, and $(x_2, y_2) = (-900m, -1000m)$, respectively. Theoretically, the DOA of T_1 relative to UAV1 and UAV2 are $\alpha_1^{(1)} = -7.125$ and $\alpha_1^{(2)} = -23.1986$, respectively, while the DOA of T_2 relative to UAV1 and UAV2 are $\alpha_2^{(1)} = -21.8014$ and $\alpha_2^{(2)} = -29.3578$. The average error (AE) is defined as

$$AE = \frac{1}{100K} \sum_{n}^{100} \left(\sqrt{\sum_{k=1}^{K} \left[(\widehat{x}_{k,n} - x_k)^2 + (\widehat{y}_{k,n} - y_k)^2 \right]} \right). \tag{39}$$

where $(\widehat{x}_{k,n}, \widehat{y}_{k,n})$ represents the estimated coordinates of the k-th target in the n-th experiment.

Table II presents the localization errors of various algorithms under 0dB and 10dB conditions. At 0dB, the localization errors of the proposed algorithm, ANM, TNNM, and OGSR algorithms are 8.1561m, 11.7696m, 10.4795m, and 12.8292m, respectively. At 10dB, the errors for these algorithms decrease to 2.2771m, 9.0738m, 9.3006m, and 3.0108m, respectively. In comparison with other algorithms, our method provides more accurate localization.

Figure 13 and figure 14 visualize the scatter distributions of the algorithms' localization results at 0dB and 10dB, respectively. Subplots (a), (b), (c), and (d) correspond to the localization results of the proposed algorithm, ANM, TNNM, and OGSR algorithms, respectively. The horizontal axis and vertical axis denote the x-coordinate and y-coordinate of the target (unit: m), respectively. We can clearly see that our method's localization results are much closer to the true positions, while the results from the other algorithms are more scattered, demonstrating the superior localization accuracy of the proposed method.

V. CONCLUSION

In this paper, a polarization-assisted UAV-borne radar localization system is developed, which utilizes a coprime EMVS array as the signal receiving device. This system overcomes the mutual coupling effects present in traditional uniform linear scalar sensor arrays and effectively exploits the polarization information of electromagnetic waves to enhance system performance. Additionally, an ANM-Tensor-DOA estimation algorithm is presented for estimating the target's DOA. Furthermore, a PACL algorithm is introduced, based

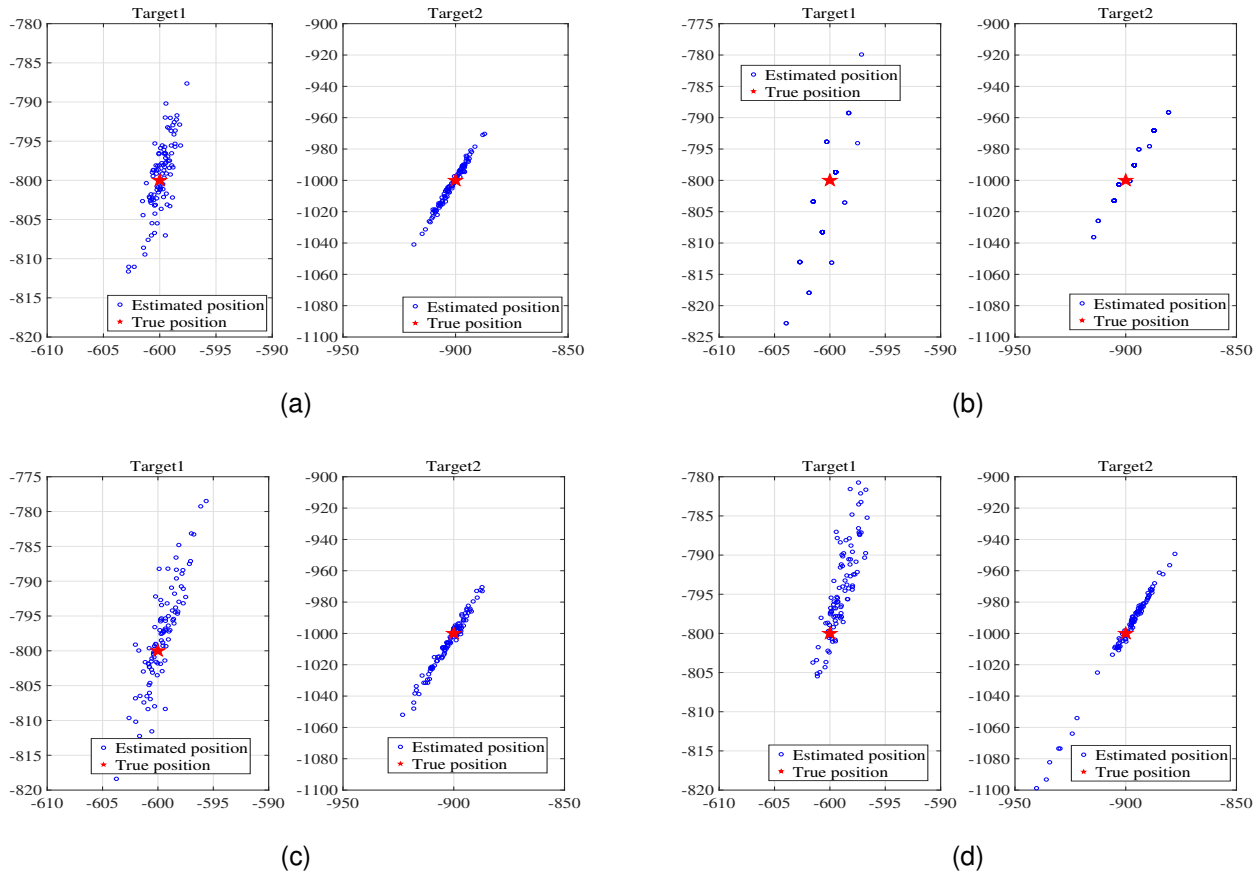

Fig. 13. Scatter distribution of localization at 0dB. (a) Proposed algorithm. (b) ANM. (c) TNNM. (d) OGSR.

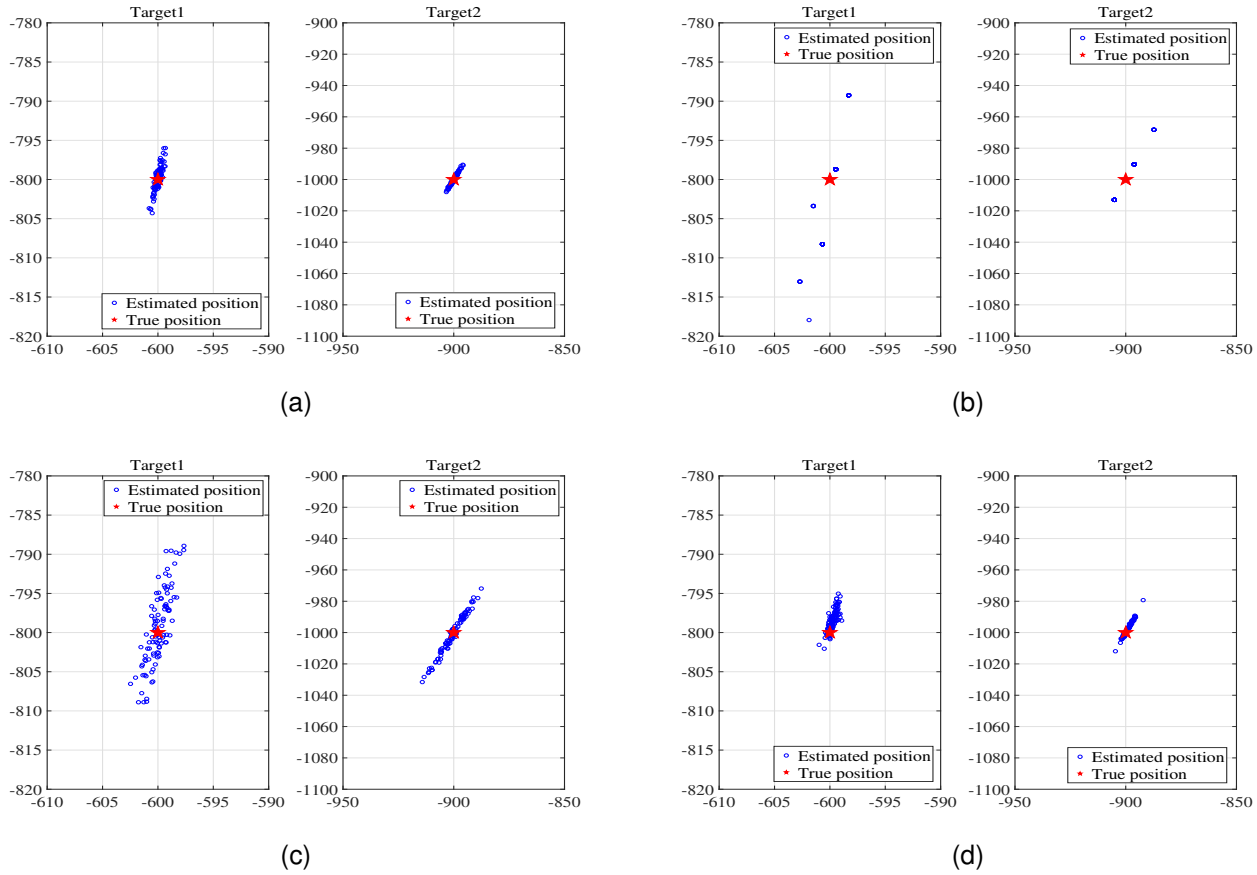

Fig. 14. Scatter distribution of localization at 10dB. (a) Proposed algorithm. (b) ANM. (c) TNNM. (d) OGSR.

on the estimated DOA, to achieve accurate target position estimation in challenging environments. In future research work, we will consider adopting the planar sparse arrays, and focus on investigating robust DOA estimation algorithms under the condition of existing array errors to further enhance the practical applicability of the proposed method.

REFERENCES

[1] M. Liu, J. Yang, and G. Gui, "DSF-NOMA: UAV-assisted emergency communication technology in a heterogeneous internet of things," *IEEE Internet Things J.*, vol. 6, no. 3, pp. 5508–5519, 2019.

[2] P. Fust and J. Loos, "Development perspectives for the application of autonomous, unmanned aerial systems (UASs) in wildlife conservation," *Biol. Conserv.*, vol. 241, p. 108380, 2020.

[3] S. Zhang, A. Ahmed, and Y. D. Zhang, "Robust source localization exploiting collaborative UAV network," in *Proc. Conf. Rec. Asilomar Conf. Signals Syst. Comput.*, Pacific Grove, CA, USA, 2019, pp. 1437–1441.

[4] S. Zhang, A. Ahmed, and Y. D. Zhang, "Sparsity-based collaborative sensing in a scalable wireless network," in *Big Data: Learning, Analytics, and Applications*, vol. 10989, Baltimore, MD, USA, 2019, pp. 18–25.

[5] H. Wang, L. Wan, M. Dong, K. Ota, and X. Wang, "Assistant vehicle localization based on three collaborative base stations via SBL-based robust DOA estimation," *IEEE Internet Things J.*, vol. 6, no. 3, pp. 5766–5777, 2019.

[6] Y. Ling, H. Gao, S. Zhou, L. Yang, and F. Ren, "Robust sparse Bayesian learning-based Off-grid DOA estimation method for vehicle localization," *Sensors*, vol. 20, no. 1, p. 302, 2020.

[7] J. Fang, H. Chen, W. Liu, S. Yang, C. Yuen, and H. C. So, "Three-dimensional localization of mixed near-field and far-field sources based on a unified exact propagation model," *IEEE Transactions on Signal Processing*, vol. 73, pp. 245–258, 2025.

[8] H. Chen, W. Zhang, L. Teng, W. Liu, S. Yang, and C. Yuen, "Robust 3-d near-field source localization method based on deep feature fusion extraction network," *IEEE Transactions on Cognitive Communications and Networking*, vol. 11, no. 6, pp. 3965–3980, 2025.

[9] H. Chen, J. Fang, W. Wang, W. Liu, Y. Tian, Q. Wang, and G. Wang, "Near-field target localization for emvs-mimo radar with arbitrary configuration," *IEEE Transactions on Aerospace and Electronic Systems*, vol. 60, no. 4, pp. 5406–5417, 2024.

[10] H. Chen, W. Wang, W. Liu, Y. Tian, and G. Wang, "An exact near-field model based localization for bistatic mimo radar with cold arrays," *IEEE Transactions on Vehicular Technology*, vol. 72, no. 12, pp. 16 021–16 030, 2023.

[11] X. Wang, L. T. Yang, D. Meng, M. Dong, K. Ota, and H. Wang, "Multi-UAV cooperative localization for marine targets based on weighted subspace fitting in SAGIN environment," *IEEE Internet Things J.*, vol. 9, no. 8, pp. 5708–5718, 2022.

[12] H. Wang, X. Wang, X. Lan, T. Su, and L. Wan, "BSBL-based auxiliary vehicle position analysis in smart city using distributed MEC and UAV-deployed IoT," *IEEE Internet Things J.*, vol. 10, no. 2, pp. 975–986, 2023.

[13] G. Han, L. Wan, L. Shu, and N. Feng, "Two novel DOA estimation approaches for real-time assistant calibration systems in future vehicle industrial," *IEEE Syst. J.*, vol. 11, no. 3, pp. 1361–1372, 2017.

[14] J. Cong, X. Wang, C. Yan, L. T. Yang, M. Dong, and K. Ota, "CRB weighted source localization method based on deep neural networks in multi-UAV network," *IEEE Internet Things J.*, vol. 10, no. 7, pp. 5747–5759, 2023.

[15] R. Akter, M. Golam, V.-S. Doan, J.-M. Lee, and D.-S. Kim, "IoMT-net: Blockchain-integrated unauthorized UAV localization using lightweight convolution neural network for internet of military things," *IEEE Internet Things J.*, vol. 10, no. 8, pp. 6634–6651, 2023.

[16] H. Chen, H. Guo, W. Liu, Q. Shen, G. Wang, and H. C. So, "Fourth-order sparse array design from a sum-difference co-array perspective," *IEEE Transactions on Signal Processing*, vol. 73, pp. 2243–2254, 2025.

[17] H. Guo, H. Chen, W. Liu, S. Yang, C. Yuen, and H. C. So, "Third-order sum-difference expansion: An array extension strategy based on third-order cumulants," *IEEE Transactions on Signal Processing*, vol. 73, pp. 2099–2109, 2025.

[18] H. Guo, H. Chen, S. Yang, W. Liu, C. Yuen, and H. C. So, "A third-order sparse array design scheme based on second-order sum-difference co-array analysis," *IEEE Transactions on Vehicular Technology*, vol. 74, no. 4, pp. 6108–6120, 2025.

[19] H. Chen, H. Lin, W. Liu, Q. Wang, Q. Shen, and G. Wang, "Augmented multi-subarray dilated nested array with enhanced degrees of freedom and reduced mutual coupling," *IEEE Transactions on Signal Processing*, vol. 72, pp. 1387–1399, 2024.

[20] H. Chen, J. Li, S. Yang, W. Liu, C. Yuen, and H. C. So, "Bilateral multi-subarray padded coprime array configuration for doa estimation in mimo radar," *IEEE Transactions on Vehicular Technology*, vol. 74, no. 8, pp. 12 714–12 726, 2025.

[21] P. Pal and P. P. Vaidyanathan, "Nested arrays: A novel approach to array processing with enhanced degrees of freedom," *IEEE Trans. Signal Process.*, vol. 58, no. 8, pp. 4167–4181, 2010.

[22] P. P. Vaidyanathan and P. Pal, "Sparse sensing with co-prime samplers and arrays," *IEEE Trans. Signal Process.*, vol. 59, no. 2, pp. 573–586, 2011.

[23] Z. Peng, Y. Ding, S. Ren, H. Wu, and W. Wang, "Coprime nested arrays for DOA estimation: Exploiting the nesting property of coprime array," *IEEE Signal Process. Lett.*, vol. 29, pp. 444–448, 2022.

[24] X. Tang, R. Hong, C. Zhu, L. Zuo, X. Qi, and Z. Xu, "DOA estimation for coprime array via Capon-MUSIC algorithm," in *2024 IEEE MTT-S Int. Wireless Symp. (IWS)*, Beijing, China, 2024, pp. 1–3.

[25] A. H. Shaikh and X. Liu, "Super fragmented coprime arrays for DOA estimation," *IEEE Signal Process. Lett.*, vol. 32, pp. 1825–1829, 2025.

[26] C.-L. Liu and P. P. Vaidyanathan, "Remarks on the spatial smoothing step in coarray MUSIC," *IEEE Signal Process. Lett.*, vol. 22, no. 9, pp. 1438–1442, 2015.

[27] P. Pal and P. P. Vaidyanathan, "Coprime sampling and the MUSIC algorithm," in *2011 Digital Signal Process. and Signal Process. Educ. Meet. (DSP/SPE)*, Sedona, AZ, USA, 2011, pp. 289–294.

[28] S. K. Yadav and N. V. George, "Fast direction-of-arrival estimation via coarray interpolation based on truncated nuclear norm regularization," *IEEE Trans. Circuits Syst. II: Express Briefs*, vol. 68, no. 4, pp. 1522–1526, 2021.

[29] C.-L. Liu, P. P. Vaidyanathan, and P. Pal, "Coprime coarray interpolation for DOA estimation via nuclear norm minimization," in *2016 IEEE Int. Symp. on Circuits and Systems (ISCAS)*, Montreal, QC, Canada, 2016, pp. 2639–2642.

[30] J. Chen, Y. Zhang, C. Yao, G. Tu, and J. Li, "Hermitian toeplitz covariance tensor completion with missing slices for angle estimation in bistatic MIMO radars," *IEEE Trans. Aerosp. Electron. Syst.*, vol. 60, no. 6, pp. 8401–8418, 2024.

[31] Y. Zhang, H. Zhou, G. Zheng, J. Shi, G. Hu, and Y. Song, "DOA estimation of coherent sources with sparse arrays via toeplitz matrix reconstruction," *IEEE Trans. Veh. Technol.*, pp. 1–14, 2025.

[32] P. Li, Y. Rui, Y. Yuan, C. Yu, P. Li, and R. Xie, "A sparse array DOA estimation approach based on matrix completion," in *2022 14th Int. Conf. on Signal Process. Syst. (ICSPS)*, Jiangsu, China, 2022, pp. 278–284.

[33] A. Nehorai and E. Paldi, "Vector-sensor array processing for electromagnetic source localization," *IEEE Trans. Signal Process.*, vol. 42, no. 2, pp. 376–398, 1994.

[34] M. R. Andrews, P. P. Mitra, and R. Decarvalho, "Tripling the capacity of wireless communications using electromagnetic polarization," *Nature*, vol. 409, no. 6818, pp. 316–318, 2001.

[35] M. Dai, X. Ma, W. Sheng, and Y. Han, "Linear dipole array with element rotation for enhanced DOA and polarization estimation," *IEEE Trans. Aerosp. Electron. Syst.*, vol. 59, no. 6, pp. 9128–9141, 2023.

[36] X. Lan, W. Liu, and H. Y. Ngan, "Joint 4-D DOA and polarization estimation based on linear tripole arrays," in *2017 22nd Int. Conf. on Digital Signal Process. (DSP)*, London, UK, 2017, pp. 1–5.

[37] X. Lan, W. Liu, and H. Y. T. Ngan, "Joint DOA and polarization estimation with crossed-dipole and tripole sensor arrays," *IEEE Trans. Aerosp. Electron. Syst.*, vol. 56, no. 6, pp. 4965–4973, 2020.

[38] P. Zhao, G. Hu, and H. Zhou, "An Off-Grid block-sparse Bayesian method for direction of arrival and polarization estimation," *Circuits, Syst., Signal Process.*, vol. 39, no. 9, pp. 4378–4398, 2020.

[39] X. Wang, X. Lan, and X. Wang, "A low-complexity sparse reconstruction algorithm of polarization-sensitive arrays," *Circuits, Syst., Signal Process.*, pp. 1–16, 2025.

[40] S. Miron, N. Le Bihan, and J. Mars, "Quaternion-MUSIC for vector-sensor array processing," *IEEE Trans. Signal Process.*, vol. 54, no. 4, pp. 1218–1229, 2006.

[41] X. Lan and W. Liu, "Fully quaternion-valued adaptive beamforming based on crossed-dipole arrays," *Electronics*, vol. 6, no. 2, p. 34, 2017.

[42] D. Meng, X. Li, and W. Wang, "Robust tensor decomposition approach for DOA estimation with EMVS-MIMO radar," *IEEE Sensors J.*, vol. 24, no. 19, pp. 31 262–31 271, 2024.
[43] F. Wen, J. Shi, and Z. Zhang, "Joint 2D-DOD, 2D-DOA, and polarization angles estimation for bistatic EMVS-MIMO radar via PARAFAC analysis," *IEEE Trans. Veh. Technol.*, vol. 69, no. 2, pp. 1626–1638, 2020.
[44] X.-P. Lin, M.-J. Zhou, L. He, C. Ge, and X.-F. Zhang, "DOA estimation of nested electromagnetic vector sensors array via MUSIC algorithm," in *2018 4th Annu. Int. Conf. on Network and Inf. Syst. for Computers (ICNISC)*, Wuhan, China, 2018, pp. 294–298.
[45] M. Fu, Z. Zheng, W.-Q. Wang, and H. C. So, "Coarray interpolation for DOA estimation using coprime EMVS array," *IEEE Signal Process. Lett.*, vol. 28, pp. 548–552, 2021.
[46] M. Fu, Z. Zheng, K. Zhang, and W.-Q. Wang, "Coarray interpolation for direction finding and polarization estimation using coprime EMVS array via atomic norm minimization," *IEEE Trans. Veh. Technol.*, vol. 72, no. 8, pp. 10 162–10 172, 2023.
[47] T. Ahmed, X. Zhang, and Z. Wang, "DOA estimation for coprime EMVS arrays via minimum distance criterion based on PARAFAC analysis," *IET Radar, Sonar & Navig.*, vol. 13, no. 1, pp. 65–73, 2019.
[48] K. Han and A. Nehorai, "Nested vector-sensor array processing via tensor modeling," *IEEE Trans. Signal Process.*, vol. 62, no. 10, pp. 2542–2553, 2014.
[49] W. Rao, D. Li, and J. Q. Zhang, "A novel PARAFAC model for processing the nested vector-sensor array," *Sensors*, vol. 18, no. 11, p. 3708, 2018.
[50] M. Fu, Z. Zheng, W.-Q. Wang, and H. C. So, "Virtual array interpolation for 2-D DOA and polarization estimation using coprime EMVS array via tensor nuclear norm minimization," *IEEE Trans. Signal Process.*, vol. 71, pp. 3637–3650, 2023.
[51] K.-C. Tan, K.-C. Ho, and A. Nehorai, "Linear independence of steering vectors of an electromagnetic vector sensor," *IEEE Trans. Signal Process.*, vol. 44, no. 12, pp. 3099–3107, 1996.
[52] X. Wang and X. Lan, "A dynamic dictionary-based sparse reconstruction method for DOA estimation," in *Proc. of the 2024 6th Int. Symp. on Signal Process. Syst.(SSPS)*, Xi'an, China, 2024, pp. 1–5.

Xiaoting Wang (Graduate Student Member, IEEE) was born in 1997. She received the M.S. degree from the School of Electronics and Information Engineering, Lanzhou Jiaotong University, Lanzhou, China, in 2022. She is currently doing her Ph.D Programme in the School of Information and Communication Engineering, Hainan University, Haikou, China.

Her current research interests include array signal processing and compressed sensing.

Xiang Lan was born in 1990. He received the B.Sc. degree from the Huazhong University of Science and Technology, China, in 2012, and the M.Sc. and Ph.D. degrees from the Department of Electronic and Electrical Engineering of the University of Sheffield, U.K., in 2014 and 2019, respectively.

From 2019 to June 2020, he worked as a Research Associate with the Department of Electronic and Electrical Engineering, the University of Sheffield. He is currently a lecturer with the School of Information and Communication Engineering, Hainan University, China. His research interests include signal processing based on vector sensor arrays (beamforming and DOA estimation with polarized signals) and sparse array processing.

Xianpeng Wang (Member, IEEE) was born in 1986. He received the M.S. and Ph.D. degrees from the College of Automation, Harbin Engineering University, Harbin, China, in 2012 and 2015, respectively. He was a full-time Research Fellow with the School of Electrical and Electronic Engineering, Nanyang Technological University, Singapore, from 2015 to 2016.

He is currently a Professor with the School of Information and Communication Engineering, Hainan University, Haikou, China. He is the author of more than 100 papers published in related journals and international conference proceedings, and was a Reviewer of more than 30 journals. His major research interests include communication system, compressed sensing, radar signal processing.

Mingcheng Fu (Member, IEEE) received the B.S. degree, M. S. degree and Ph. D. degree in communication engineering from the University of Electronic Science and Technology, Chengdu, China, in 2016, 2019, and 2024, respectively. He is currently a Lecturer with the School of Information and Communication Engineering, Hainan University, China. His research interests include array signal processing, especially direction-of-arrival estimation, polarization estimation, robust adaptive beamforming, and source localization, wireless communications, and signal processing for conformal arrays.